CONTRACT TECHNICAL REPORT

"Three Dimensional Effects in Fiber Reinforced Composites Under Compression"

By

S. Xu and Y. Jack Weitsman

Prepared for: Office of Naval Research
Arlington, Virginia

Mechanics Division
Engineering Science Directorate
Contract N00014-90-J-1556

Report ESM95-2.0-CM
February 1995

Engineering Science and Mechanics
THE UNIVERSITY OF TENNESSEE
Knoxville, TN 37996-2030

Unclassified

SECURITY CLASSIFICATION OF THIS PAGE

REPORT DOCUMENTATION PAGE

1a. REPORT SECURITY CLASSIFICATION: Unclassified	1b. RESTRICTIVE MARKINGS
2a. SECURITY CLASSIFICATION AUTHORITY	3. DISTRIBUTION/AVAILABILITY OF REPORT: Unlimited
2b. DECLASSIFICATION/DOWNGRADING SCHEDULE	
4. PERFORMING ORGANIZATION REPORT NUMBER(S)	5. MONITORING ORGANIZATION REPORT NUMBER(S)
6a. NAME OF PERFORMING ORGANIZATION: Eng. Science & Mechanics, University of Tennessee; 6b. OFFICE SYMBOL (If applicable)	7a. NAME OF MONITORING ORGANIZATION: Office of Naval Research
6c. ADDRESS (City, State and ZIP Code): 307 Perkins Hall, Knoxville, TN 37996-2030	7b. ADDRESS (City, State and ZIP Code): Office of Naval Research, Code 432, 800 N. Quincy Ave., BCT # 1, Room 528, Arlington, VA 22217
8a. NAME OF FUNDING/SPONSORING ORGANIZATION: Office of Naval Research; 8b. OFFICE SYMBOL (If applicable)	9. PROCUREMENT INSTRUMENT IDENTIFICATION NUMBER: N00014-90-J-1556 (ONR Contract #)
8c. ADDRESS (City, State and ZIP Code): Arlington, VA 22217	10. SOURCE OF FUNDING NOS. — PROGRAM ELEMENT NO. / PROJECT NO. / TASK NO. / WORK UNIT NO.
11. TITLE (Include Security Classification): Three Dimensional Effects in Fiber Reinforced Composites Under Compression	
12. PERSONAL AUTHOR(S): S. Xu and Y. Jack Weitsman	
13a. TYPE OF REPORT: Technical; 13b. TIME COVERED: FROM 10/1/92 TO 2/2/95	14. DATE OF REPORT (Yr., Mo., Day): 95-02-02; 15. PAGE COUNT: 25
16. SUPPLEMENTARY NOTATION	
17. COSATI CODES — FIELD / GROUP / SUB. GR.	18. SUBJECT TERMS (Continue on reverse if necessary and identify by block number)

19. ABSTRACT (Continue on reverse if necessary and identify by block number)

This article demonstrates that the stress and displacement fields in composites reinforced by hexagonal fiber arrays differ both qualitatively and quantitatively from results obtained for fiber and matrix layers. The layered representation is a commonly used approximation for analyzing the compressive response of composites.

Finite element computational results are presented for the mechanical fields in uni-axially reinforced fibrous composites subjected to compression parallel to the fiber direction. The fibers are assumed to deflect in a shearing mode deformation and both linear and non-linear responses are considered for the matrix material.

The results exhibit a pronounced three dimensional character, with significant stress concentrations near the fiber/matrix interfaces and shear stresses τ_{yz} of magnitudes equivalent to those of τ_{xz}. All these features are disregarded by the layered model and may account for its inadequacy in predicting compressive failure.

20. DISTRIBUTION/AVAILABILITY OF ABSTRACT: UNCLASSIFIED/UNLIMITED ☐ SAME AS RPT. ☐ DTIC USERS ☐	21. ABSTRACT SECURITY CLASSIFICATION: Unclassified
22a. NAME OF RESPONSIBLE INDIVIDUAL: Dr. Yapa Rajapakse	22b. TELEPHONE NUMBER (Include Area Code): (703) 696-4405; 22c. OFFICE SYMBOL

DD FORM 1473, 83 APR EDITION OF 1 JAN 73 IS OBSOLETE.

SECURITY CLASSIFICATION OF THIS PAGE

Unclassified

Three Dimensional Effects in Fiber Reinforced Composites Under Compression

by

S. Xu and Y. Weitsman

Abstract

This article demonstrates that the stress and displacement fields in composites reinforced by hexagonal fiber arrays differ both qualitatively and quantitatively from results obtained for fiber and matrix layers. The layered representation is a commonly used approximation for analyzing the compressive response of composites.

Finite element computational results are presented for the mechanical fields in uni-axially reinforced fibrous composites subjected to compression parallel to the fiber direction. The fibers are assumed to deflect in a shearing mode deformation and both linear and non-linear responses are considered for the matrix material.

The results exhibit a pronounced three dimensional character, with significant stress concentrations near the fiber/matrix interfaces and shear stresses τ_{yz} of magnitudes equivalent to those of τ_{xz}. All these features are disregarded by the layered model and may account for its inadequacy in predicting compressive failure.

Introduction

With very few exceptions, the modelling of the compressive response of fiber-reinforced composites is based upon the proposition that fiber and matrix regions can be represented as layered domains. This simplification enabled Rosen [1] to predict compressive failure by means of a classical buckling analysis and has been followed by the great majority of investigators since. Detailed listings of references can be found in the articles of Shuart [2], Camponeschi [3], Guynn et al. [4] and Piggott [5]. The above mentioned exceptions, all employing linear elasticity, occur in the analyses of Sadowsky et al. [6], Hermann et al. [7], Lanir and Fung [8] and Greszczuk [9], where the circular shape of the fiber cross-section was recognized in various contexts. With the exception of Greszczuk, the foregoing articles consider a single fiber, while the complexity arising from the circular reinforcement geometry is simplified by Greszczuk by means of an assumed shape function.

All the above models are deficient to various degrees in predicting the compressive failure of fibrous composites. Most predict failures at load levels which exceed experimental observations and all predict compressive failure loads which increase monotonically with fiber volume fraction V_f. The latter prediction is negated by experimentally observed trends [10] and [11]*.

The main purpose of the present article is to demonstrate that the complexities and intricacies of the stress field in fiber reinforced composites subjected to compression cannot be represented by models which employ layered geometries. Such models err in two major aspects: (a) they overlook high local stress concentrations, especially near the fiber matrix interfaces, and (b) they account for only one shear stress in the matrix (τ_{xz}) while discarding a second component (τ_{yz}) which is of an equivalent magnitude. These inadequacies were noted in a recent work [13], by means of an idealized, linear elastic formulation.

---

* In a recent article [12], an improved correlation between compressive failure stress and V_f was achieved by considering non-uniform fiber spacings. However, that work still employed the prevailing approximation of layered domains.

An impressive and conclusive experimental evidence for the existence of local stress concentrations and of three dimensional features arising in fibrous composites under compression was provided in a recent work by Lankford [14]. Typical observations which exhibit the foregoing effects are shown in Figure 1.

Basic Considerations

Consider a composite material, uni-directionally reinforced by a perfect hexagonal fibrous array extending in the x-y plane as shown in Figure 2a. Let the fibers run parallel to the z direction, with compression applied in the fiber direction. Due to symmetry it suffices to analyze the representative rectangular area PQRS shown in Figure 2b.

For graphite/PEEK (APC-2) composites with fiber volume fraction $V_f = 0.4$ we have a = 4μm and b = 6μm in Figure 2b. In addition, we presume a lateral deflection that varies sinusoidally in z with waviness length 2L, where L = 800a. Such waviness, sketched in Figure 3a, is attributable to processing non-uniformities, as reported by several investigators [15] and [16]. Consequently, it is possible to confine the computations to the rectangular block - $L/2 \le z \le L/2$ with the cross-sectional area shown in Figure 3b.

The computations assumed isotropic fiber and employed values of $E_f = 214$ GPa, and $\nu_f = 0.3$. The one dimensional non-linear shear response of the matrix shown by curve "a" in Figure 4 [15] was expressed by the relation $\gamma = \tau/A + (\tau/B)^q$, where A = 3096, B = 169.93, and q = 4.2 (A, B and τ in MPa). The above expression was extended to the three dimensional case by means of the Von-Mises criterion. Accordingly, the relation between the effective strain ε_e and effective stress σ_e is given by letting $\varepsilon_e = \frac{2}{\sqrt{3}}\gamma$ and $\sigma_e = \sqrt{3}\tau$ in the foregoing expression. The resulting relation among effective quantities is shown by the curve "e" in Figure 4.

To assess the significance of the non-linear matrix response, comparative computations were performed for an assumed isotropic linear elastic matrix behavior with $E_m = 6.5$ GPa and $\nu_m = 0.3$.

In addition to the foregoing sets of stress-strain relations within the fiber and the matrix regions, and the obvious requirement of stress equilibrium which are incorporated within the finite element code, we

utilized the following boundary conditions for the representative block $0 \le x \le \sqrt{3}\, b$, $0 \le y \le b$, $-L/2 \le z \le L/2$:

$$\begin{aligned} &v = 0,\ \tau_{xy} = 0,\ \tau_{yz} = 0 && \text{on } y = 0 \text{ and } y = b \\ &u = u_0 \sin(\pi z/L),\ v = 0,\ w = -z\varepsilon_z^0 && \text{on } x = 0 \text{ and } x = \sqrt{3}\, b \\ &w = \pm (L/2)\varepsilon_z^0,\ \tau_{xz} = 0,\ \tau_{yz} = 0 && \text{on } z = \pm L/2 \end{aligned} \tag{1}$$

where all symbols in equations (1) accord with standard notation.

The uniform compressive strain ε_z^0 in equations (1) is given by $\varepsilon_z^0 = \frac{\Delta}{L/2}$, where Δ denotes the deflection of the plane $z = L/2$ relative to $z = 0$, given by

$$\Delta = \frac{1}{2}\int_0^{L/2} \left(\frac{\partial u}{\partial z}\right)^2 dz = \frac{\pi^2}{8L} u_0^2 \tag{2}$$

Upon selecting $u_0 = 8a$ the computations corresponded to a compressive strain

$$\varepsilon_z = \varepsilon_z^0 = \frac{\pi^2}{4}\left(\frac{u_0}{L}\right)^2 \tag{3}$$

Computational Details

In view of the high slenderness ratio, L/b, of the representative rectangular block the computational scheme employed a coarse mesh to cover the entire representative region, and a refined mesh to focus on the region $-2a < z < a$.

The coarse mesh consisted of 800 layers normal to the z direction, with each layer further subdivided into 16 area elements as shown in Figures 5a and 5b. Figure 5a also shows the deformed configuration of the representative block with the coarse finite elements mesh. In the coarse mesh depicted in Figure 5b each fiber is contained within the three elements at the upper right and lower left corners.

The stress and displacement fields were computed through the implementation of the commercial code ABAQUS Version 5.2, using SUN Sparcstations. The computations implemented the Von-Mises plasticity model with an assumed isotropic hardening. The resulting contours of the displacement component w at $z = 0$ are shown in Figure 6, while values of the displacement components u and v at selected (x, y) locations and at $z = 0$ are listed in Table 1. It is obvious that the contours in Figure 6 exhibit strong variations in both x and y directions and that the displacement v attains amplitudes comparable to those of u. Both observations demonstrate significant departures from results predicted for layered geometries.

To focus attention on the stress and displacement fields at the mid-plane $z = 0$, where they attain maximal amplitudes, the region $-2a \le z \le a$ was subdivided by a finer mesh into 30 layers normal to z, with each layer consisting of 116 elements as shown in Figure 7. The refined mesh allots each fiber 39 elements adjacent to the upper right and lower left corners in that figure.

The asymmetry in the range of z about $z = 0$ in the refined mesh was chosen deliberately to assess the adequacy of the selected range $-2a \le z \le a$. This assessment is provided by examining the magnitudes of relative deviations in computed values from the obvious requirements of symmetry about rays emanating from the central point $x = \sqrt{3}\, b/2$, $y = b/2$. (The above range turned out to be adequate since the computational results met those requirements to a high degree of accuracy).

Accordingly, the displacements computed with the coarse mesh at $z = -2a$ and $z = a$, as well as their interpolated values at locations x, y which matched positions on the refined mesh, were employed as prescribed boundary values for the detailed computation. For purpose of illustration, the boundary values of w (x, y) at $z = a$ are sketched in Figure 8.

Comparisons with predictions derived for layered geometries were obtained by considering a rectangular block $-L/2 \le z \le L/2$ with an inner "matrix layer" and outer "fiber layers" contained within $0 \le x \le t/2$, $\sqrt{3}\, b - t/2 \le x \le \sqrt{3}\, b$, $0 \le y \le b$, respectively, as shown in Figure 9. The equality of V_f requires that $t = \frac{\pi a^2}{2b}$. The deformed shape of the layered geometry is shown in Figure 10.

Results and Discussion

Contours of the displacement w and the stresses τ_{xz}, τ_{yz} and σ_z are shown in Figures 11 and 12 for the linear case and in Figure 13 for the non-linear matrix response depicted in Figure 4.

Figures 11 and 13 exhibit contours of the above mentioned components at the mid-plane z = 0 while Figure 12 provides perspective views of the deformed blocks between z = - a and z = a/2. For additional clarity the displacements w(x, 0 , 0) and w(x, b, 0) are plotted vs. $(0 < x < \sqrt{3}\, b)$ in Figures 14a and 14b.

The results shown in Figures 11 through 14 are contrasted against predictions which correspond to layered "fiber" and "matrix" regions shown in Figures 15 and 16. Comparative values of the largest stress components are given in Table 2. That table lists values for circular and layered geometries, denoted by rows labeled "C" and "L", respectively, and contains comparisons between linear and plastic matrix response.

The predominant conclusions to be drawn from the current results are:

(1) It is erroneous to represent fibrous arrays of fiber reinforced materials by equivalent layered media for evaluating compressive response.

(2) The stress and displacement fields in fibrous arrays subjected to compression are markedly non-uniform and exhibit highly localized effects, especially near the fiber/matrix interfaces.

(3) The shear stress τ_{yz}, which is disregarded in the layered representation, attains magnitudes which are equivalent to those of τ_{xz}.

(4) Compressive failure of fiber reinforced composites may arise due to localized effects which are overlooked by the layered model.

Acknowledgement

This work was performed under Contract N00014-90-J-1556 from the Office of Naval Research to one of the authors (YW). The authors wish to thank the program manager, D. Y. Rajapakse of the Mechanics Division, Engineering Sciences Directorate, for his encouragement and support.

References

[1] Rosen, B. W., (1965). "Mechanics of composite strengthening," *Fiber Composite Materials*, American Society for Metals, pp. 37-75.

[2] Shuart, M. J., (1985). "Short-wavelength buckling and shear failures for compression-loaded composite laminates," *NASA TM 87640*.

[3] Camponeschi, Jr., E. T., (1991). "Compression of composite materials: a review," *Composite Materials: Fatigue and Fracture*, ASTM STP 1110, pp. 550-578.

[4] Guynn, E. G., Ochoa, O. O., and Bradley, W. L., (1992). "A parametric study of variables that affect fiber microbuckling initiation in composite laminates: part 1 analyses," *Journal of Composite Materials*, Vol. 26, pp. 1594-1616.

[5] Piggott, M. R., (1993). "Compressive strength of composites: how to measure it and how to improve it," *Proceedings of the International Conference on Advanced Composite Materials*, pp. 51-59. Wollongong, Australia February 15-19, 1993.

[6] Sadowsky, M. A., Pu, S. L., and Hussain, M. A., (1967). "Buckling of microfibers," *Journal of Applied Mechanics*, Vol. 34, pp. 1011-1016.

[7] Hermann, L. R., Mason, W. E., and Chan, S. T. K., (1967). "Response of reinforcing wires to compressive states of stress," *Journal of composite Materials*, Vol. 1, pp. 212-226.

[8] Lanir, Y. and Fung, Y. C. B., (1972). "Fiber composite columns under compression," *Journal of Composite Materials*, Vol. 6, pp. 387-401.

[9] Greszczuk, L. B., (1975). "Microbuckling failure of circular fiber-reinforced composites," *AIAA J.*, Vol. 13, pp. 1311-1318.

[10] Piggott, M. R. and Harris, B., (1990). "Compression strength of carbon, glass and Kevlar-49 fibre reinforced polyester resins," *Journal of Materials Science*, Vol. 15, pp. 2523-2538.

[11] Morley, J. G., (1987). *High Performance Fiber Composites*, Academic Press.

[12] Chung, I. and Weitsman, Y., (1995). "On the buckling/kinking compressive failure of fibrous composites," *International Journal of Solids and Structures*. (In print)

[13] Weitsman, Y. and Chung, I., (1994). "Can the compressive response of fiber-reinforced composites be modelled by layered arrays?" University of Tennessee Technical Report ESM 94–1.0–CM.

[14] Lankford, J., (1991). "Compressive damage and failure at high loading rates in graphite fiber-reinforced polymeric matrix composites," *Ceramic Transaction, Vol. 19, Advanced Composite Materials*, (Ed., M. D. Sacks), The American Ceramic Society, Westerville, OH, pp. 553-563.

[15] Kyriakides, S., Perry, E. J., and Liechti, K. M., (1994). "Instability and failure of fiber composites in compression," in *Mechanics USA 1994*. Proceedings of the Twelfth US National Congress of Applied Mechancis, June 1994, Seattle, Washington. (Ed., A. S. Kobayashi). Applied Mechanics Reviews, Vol. 47, No. 6, Part 2, pp. S262-S268.

[16] Bhalerao, M. and Moon, T., (1994). "On the growth-of-waviness in fiber-reinforced polymer composites: viscoelastic bifurcation and interfacial sensitivity," *Mechanics of Materials Processing and Manufacturing*, ASME AMD-192, pp. 361-385.

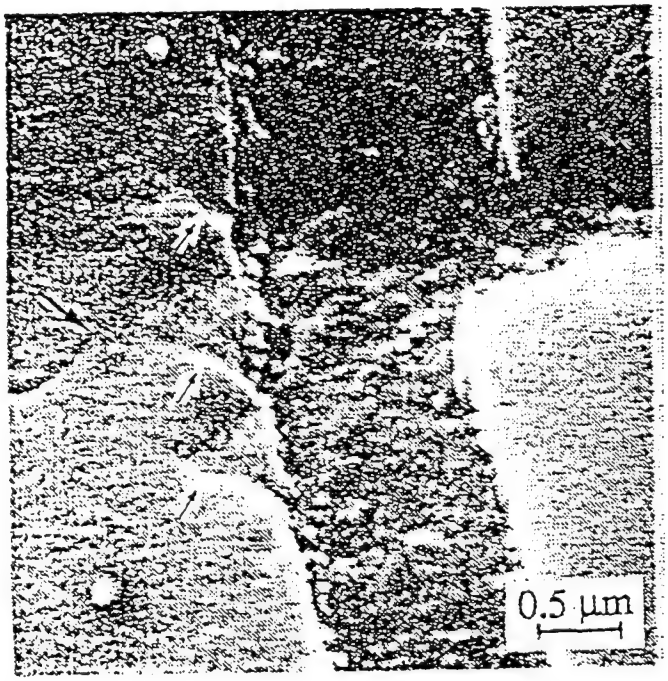

Fig. 1. A detailed exposition of the compressive deformation of fibrous composites. Note the multiple compressive deformation bands (small arrows) and the arrested crack tip (large arrow) in the fiber on the right and the fracture in the left fiber. The central matrix region exhibits significantly non-uniform deformations, with possible interfacial separation. Lankford, Ref. [14], Figure 7a. Reprinted by permission of The American Ceramic Society.

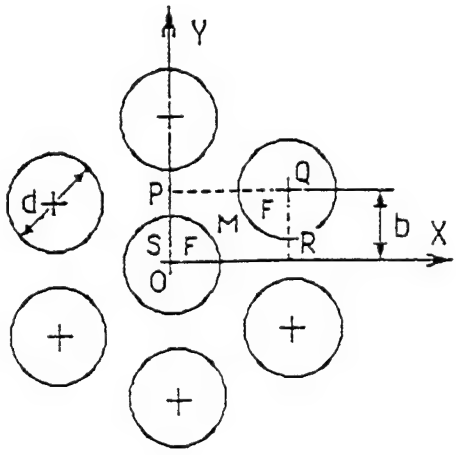

Fig. 2a. Hexagonally arrayed fibers.

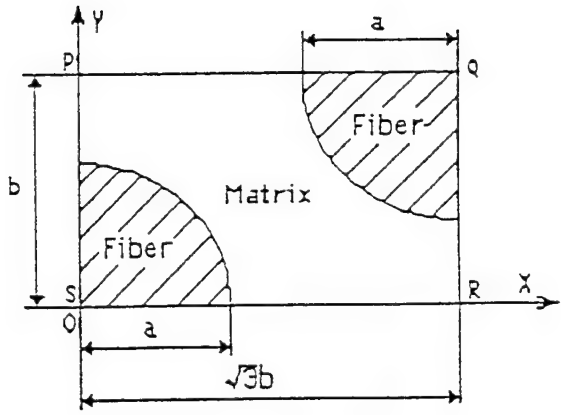

Fig. 2b. The representative cross-section of the hexagonal array.

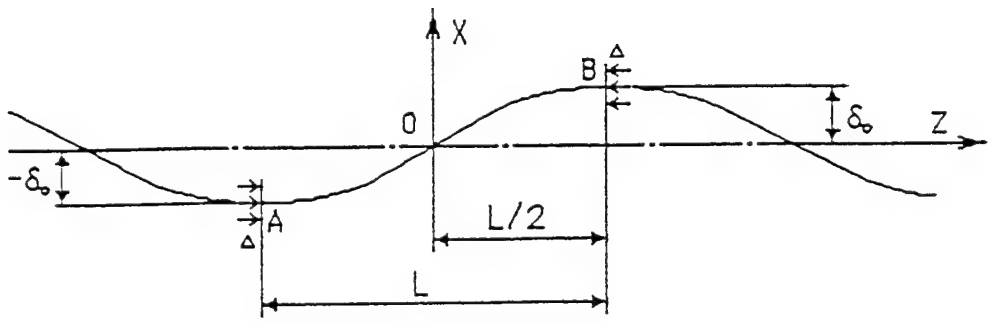

Fig. 3a. A sketch of fiber waviness.

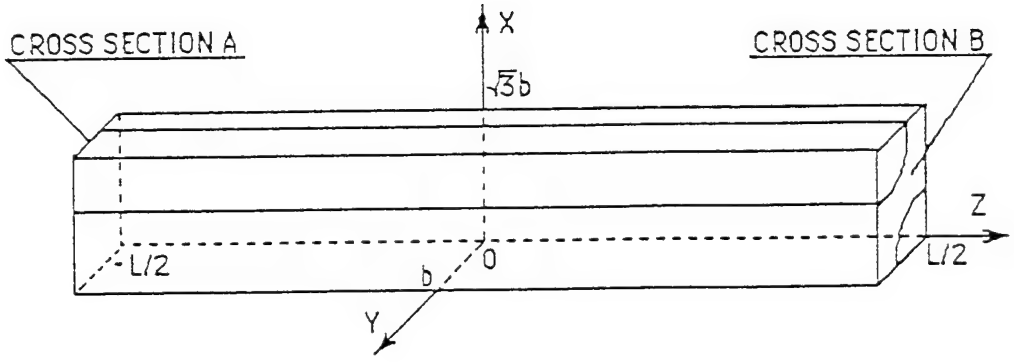

Fig. 3b. The representative volumetric block.

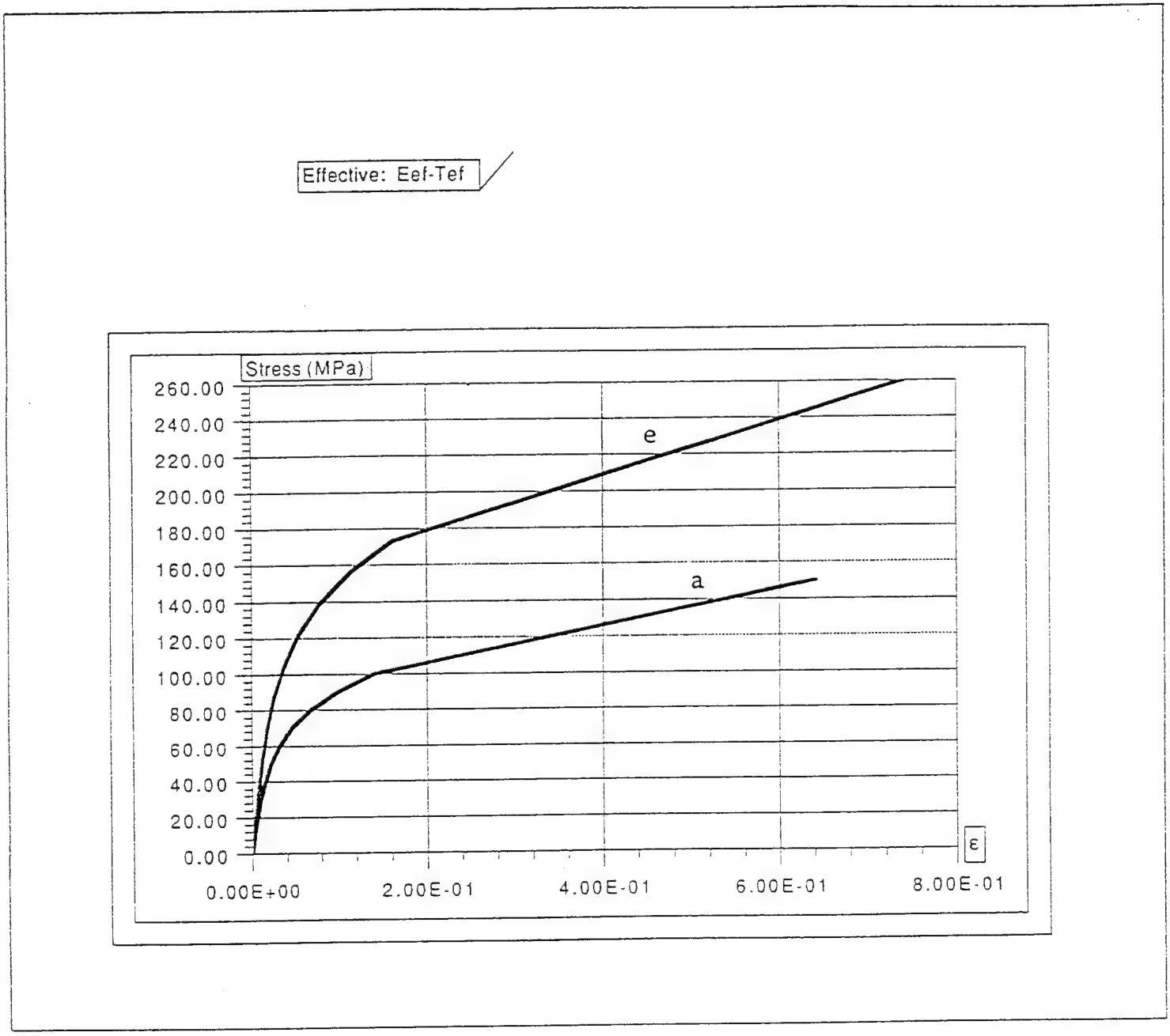

Fig. 4. The in-situ non-linear shear stress-strain response of PEEK (curve "a") and its extension to the three dimensional case in terms of effective stress and strain (curve "e").

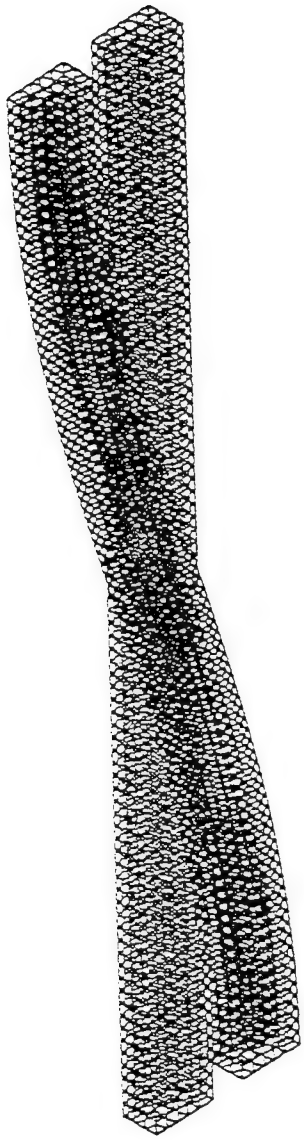

Fig. 5a. Deformation overview and coarse mesh geometry.

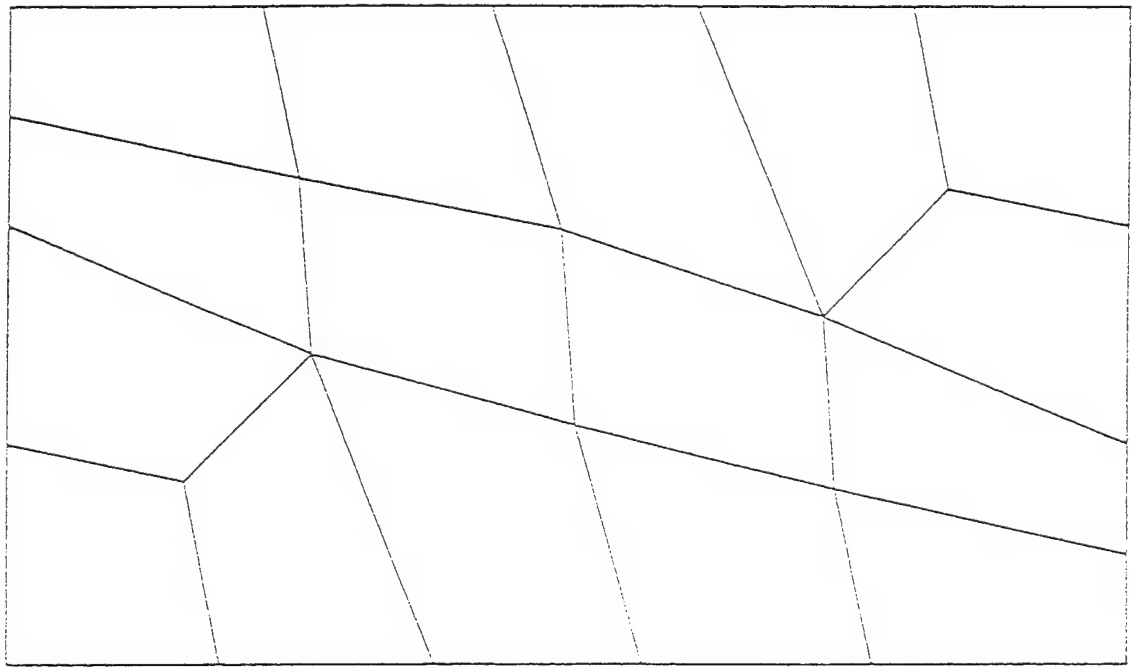

Fig. 5b. The cross-sectional coarse mesh.

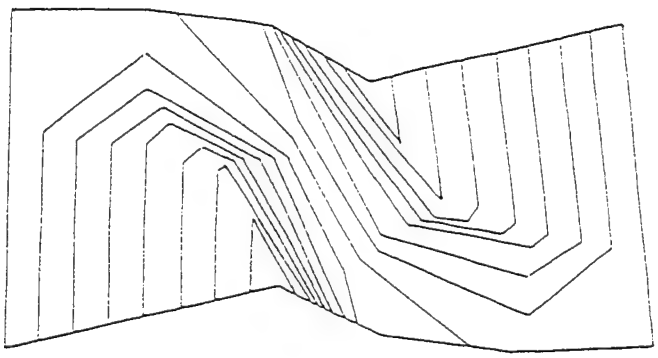

Fig. 6. Contours of the displacement w at the mid-plane z = 0 computed with the coarse mesh.

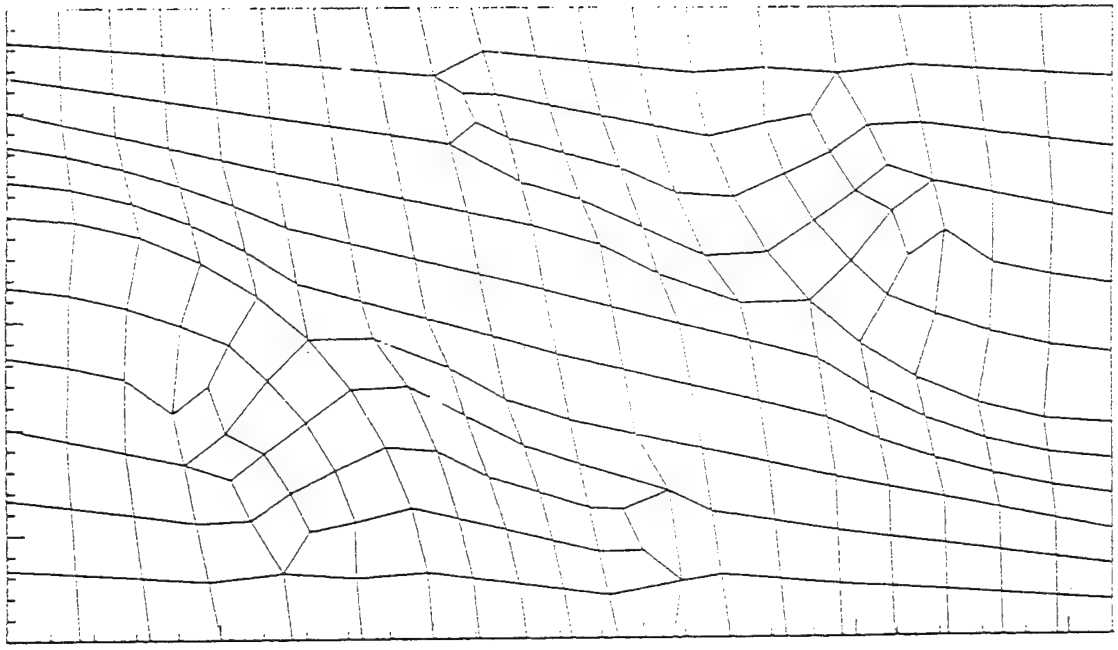

Fig. 7. The cross-sectional fine mesh. The fiber regions are covered by 39 elements near the upper right and lower left corners.

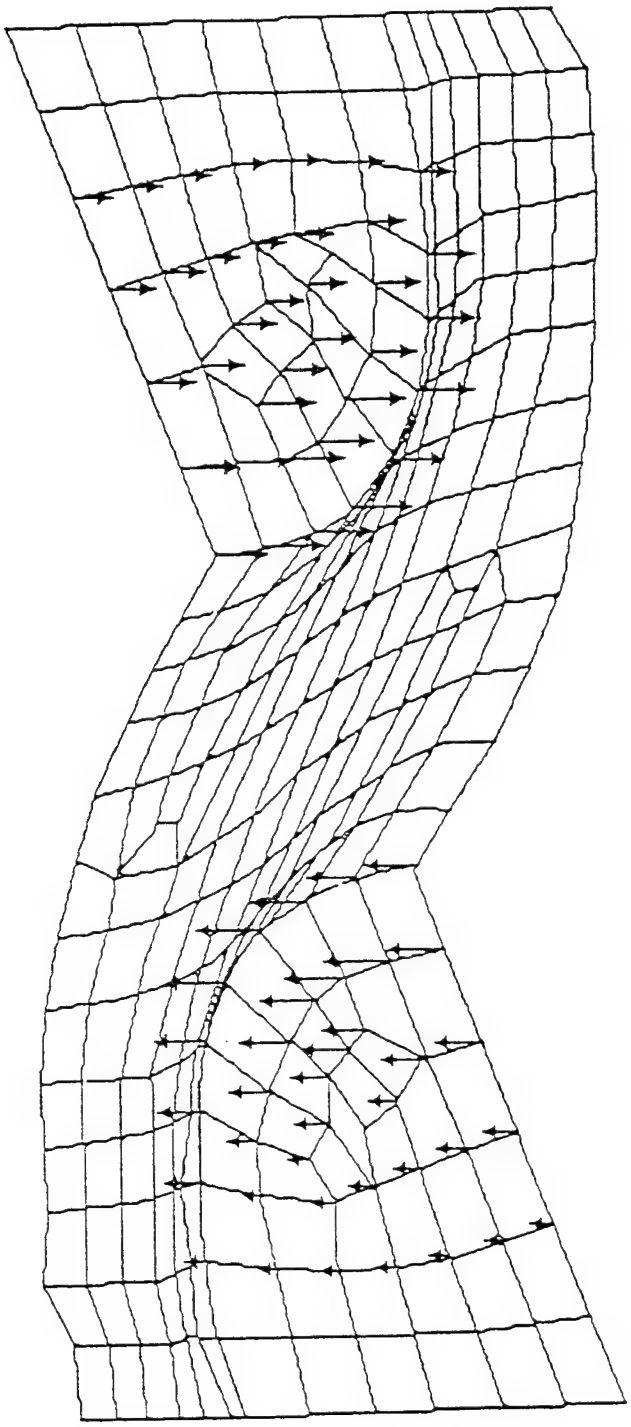

Fig. 8. A sketch of the distributed nodal displacements, computed with the coarse model, applied as boundary conditions of the top surface of the fine mesh.

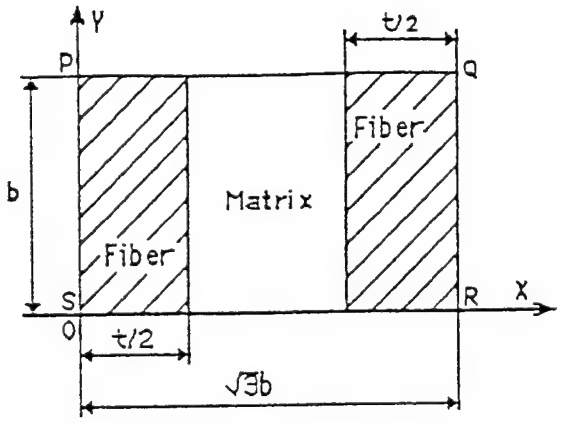

Fig. 9. The equivalent layered fiber/matrix geometry.

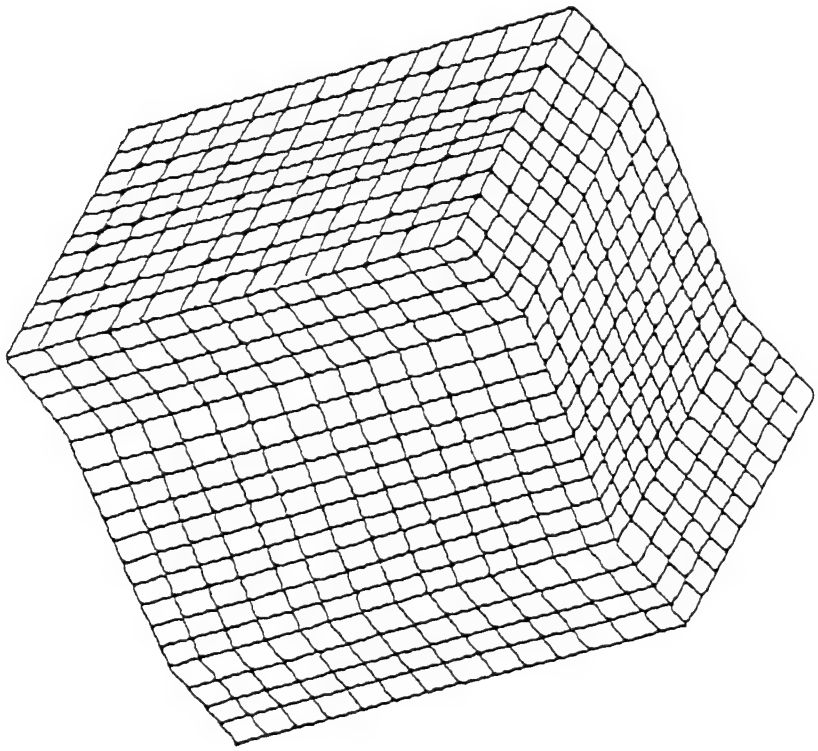

Fig. 10. The deformed shape of the layered geometry under analogous compressive circumstances.

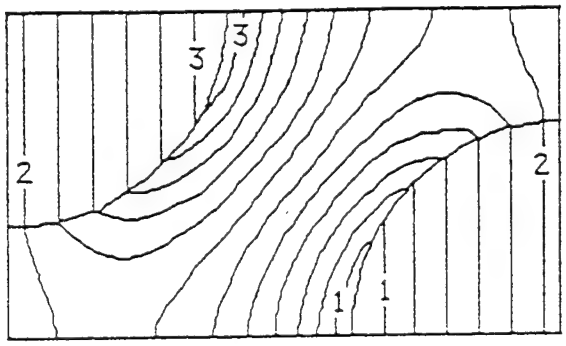

(a) The displacement w
Contours "1", "2", and "3" correspond to w = - 9.65 x 10^{-8}, 8.35 x 10^{-9}, and 9.57 x 10^{-8} m, respectively.

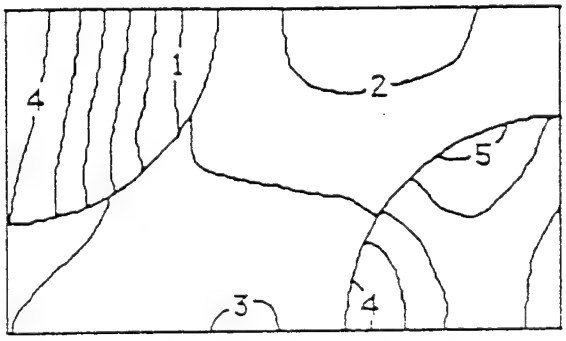

(b) Normal stress σ_{zz}
Contours "1", "2", and "3" correspond to σ_{zz} = - 27.7, 1.35, and 10.3 MPa, respectively.

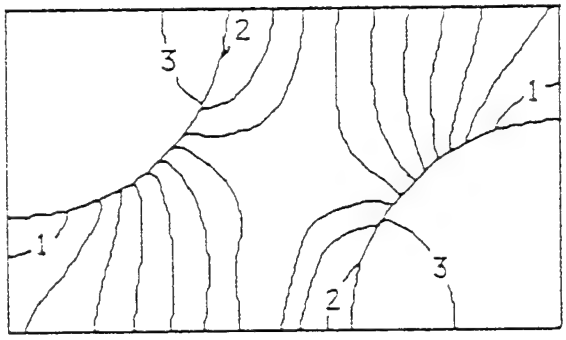

(c) Shear stress τ_{xz}
Contours "1", "2", and "3" correspond to τ_{xz} = 35.4, 209, and 248 MPa, respectively.

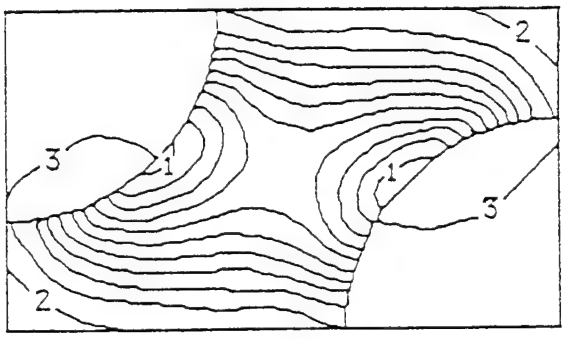

(d) Shear stress τ_{yz}
Contours "1", "2", and "3" correspond to τ_{yz} = - 2.11, 7.3, and 101 MPa, respectively.

Fig. 11. Linear results: Displacement and stress contours in the mid plane (z = 0) with circular fibers geometry.

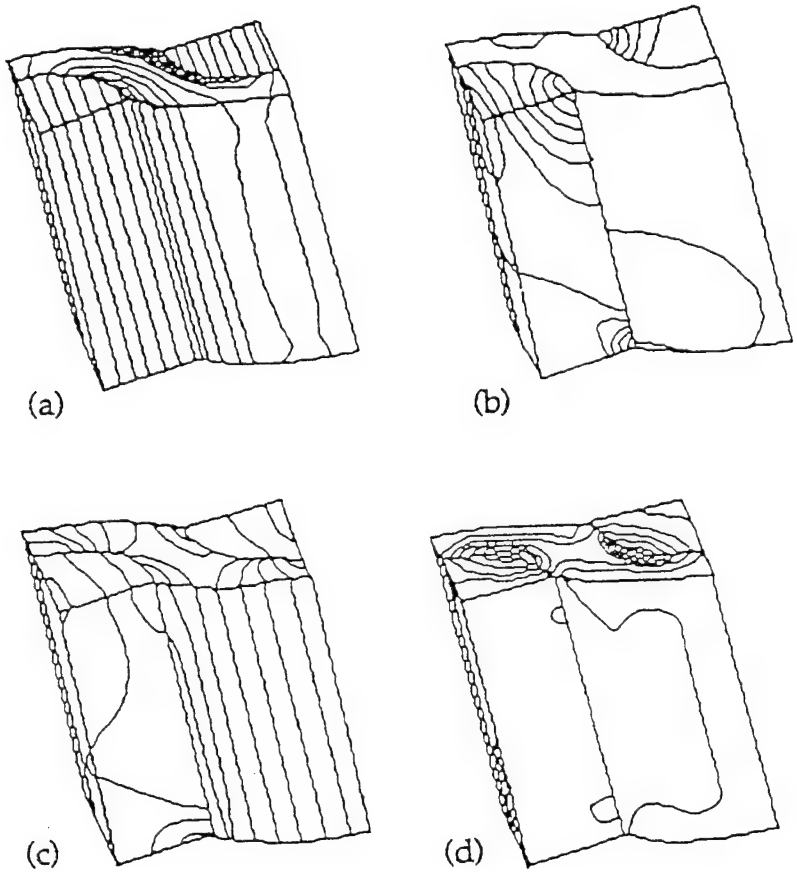

Fig. 12. Displacement and stress contours in the region - $2a \leq z \leq a$. Linear elastic results employing the fine mesh.
(a) The displacement w (b) σ_{zz} (c) τ_{xz} (d) τ_{yx}.

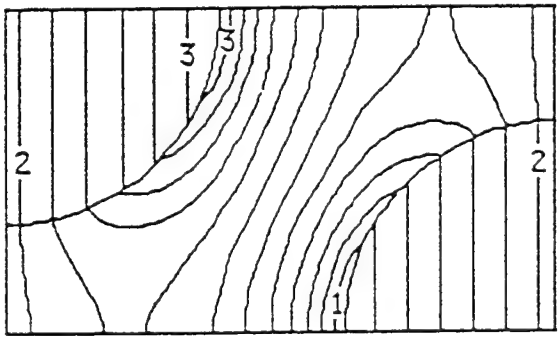

(a) The displacement w
Contours "1", "2", and "3" correspond
to $w = -1 \times 10^{-7}, 9.43 \times 10^{-9}$, and
1×10^{-7} m, respectively.

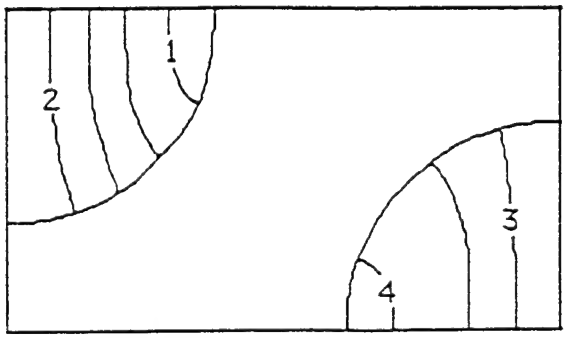

(b) Normal stress σ_{zz}
Contours "1", "2", "3", and "4" correspond
to $\sigma_{zz} = -15.2, -15.9, 93.3$, and
147 MPa, respectively.

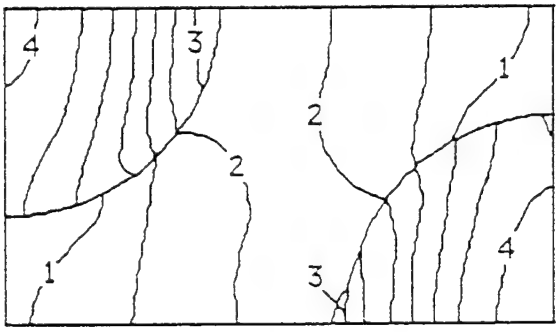

(c) Shear stress τ_{xz}
Contours "1", "2", "3", and "4" correspond
to $\tau_{xz} = 24.6, 55.0, 100.0$, and
19.2 MPa, respectively.

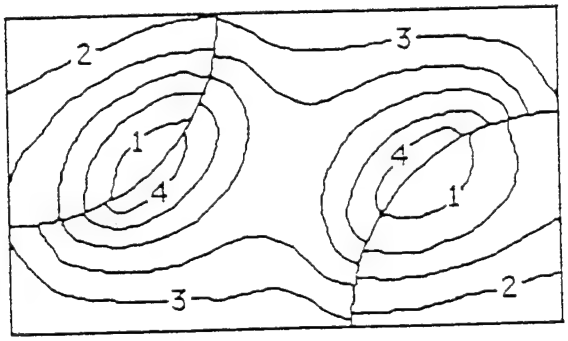

(d) Shear stress τ_{yz}
Contours "1", "2", "3", and "4" correspond
to $\tau_{yz} = -35.8, -6.1, 5.82$, and
29.6 MPa, respectively.

Fig. 13. Nonlinear results: Displacement and stress contours in the mid plane (z = 0) with circular fiber geometry.

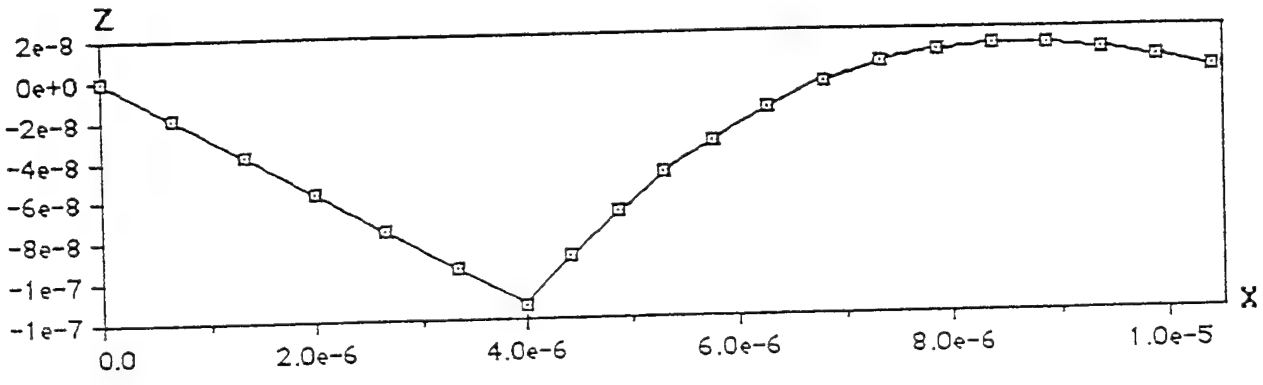

Fig. 14a. The displacement w vs. X at z = 0, y = 0.

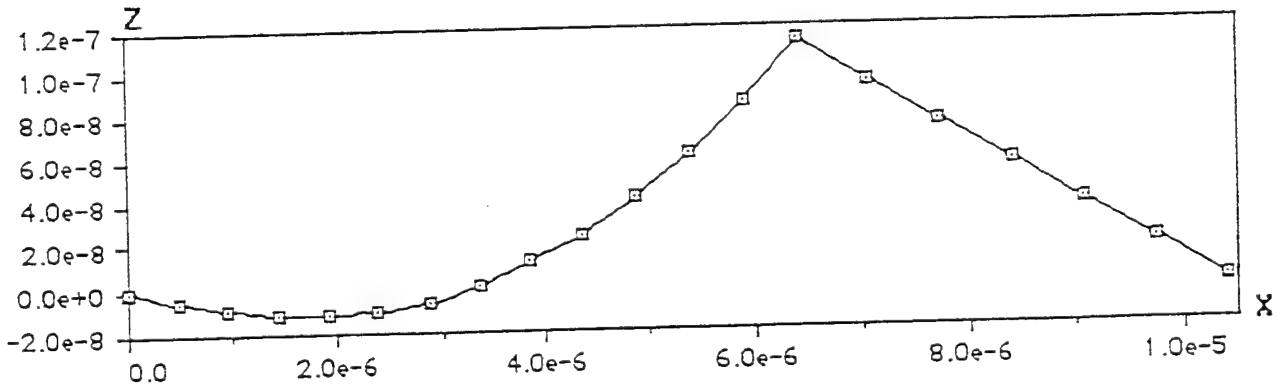

Fig. 14b. The displacement w vs. X at z = 0, y = b.

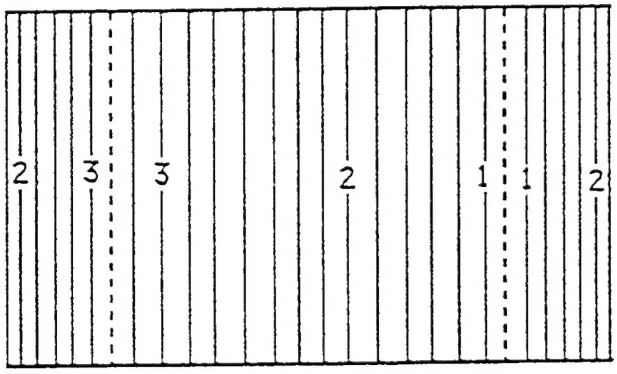

(a) The displacement w
Contours "1", "2", and "3" correspond to $w = -5.3 \times 10^{-8}$, 4.7×10^{-9}, and 5.28×10^{-8} m, respectively.

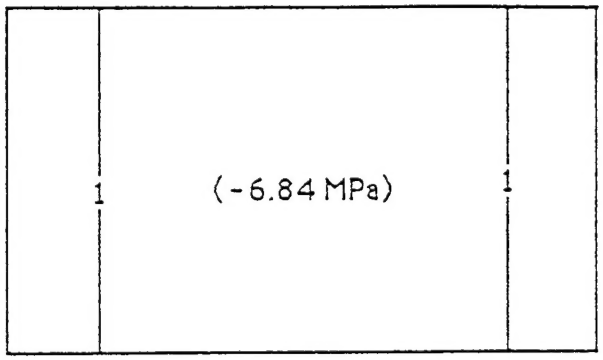

(b) Normal stress σ_{zz}
Contour "1" corresponds to $\sigma_{zz} = -69.9$ MPa.

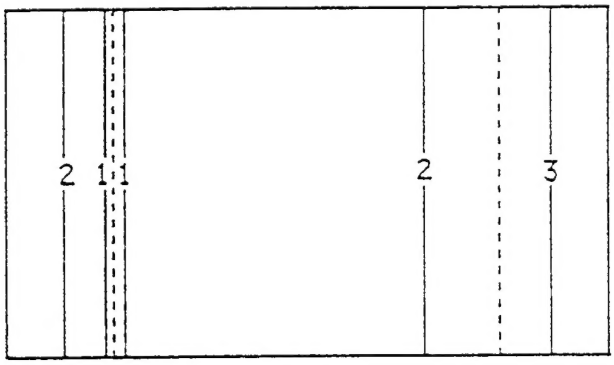

(c) Shear stress τ_{xz}
Contours "1", "2", and "3" correspond to $\tau_{xz} = 128$, 129, and 130 MPa.

Fig. 15. Linear results: Displacement and stress contours in the mid plane of the layered geometry.

[Note: The dashed lines represent the interfaces between "fiber" and "matrix" layers.]

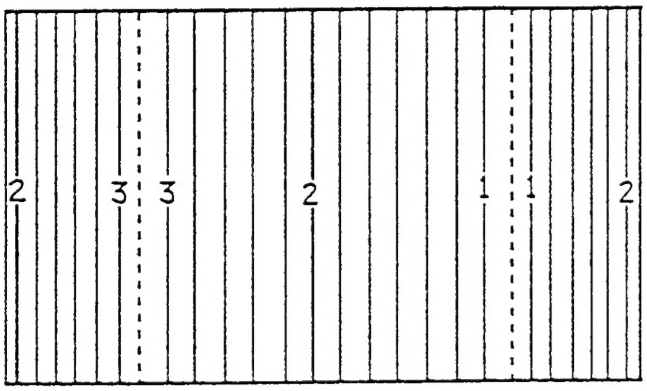

(a) The displacement w
Contours "1", "2", and "3" correspond to w = - 5.44 x 10^{-8}, 5.0 x 10^{-9}, and 5.42 x 10^{-8} m, respectively.

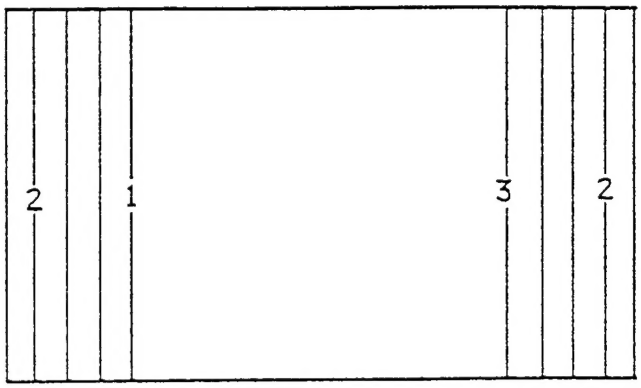

(b) Normal stress σ_{zz}
Contours "1", "2", and "3" correspond to σ_{zz} = - 103, - 60.2, and 8.82 MPa, respectively.

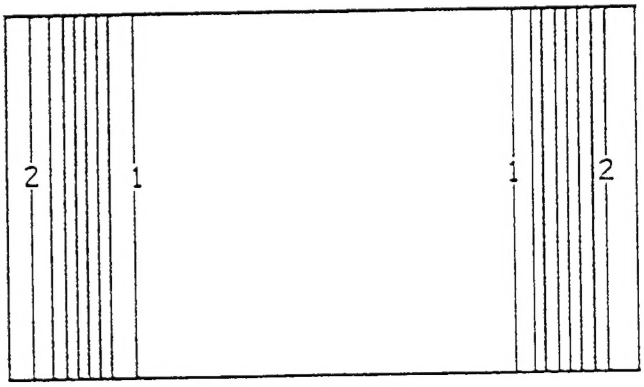

(c) Shear stress τ_{xz}
Contours "1" and "2" correspond to τ_{xz} = 52.7 and 77.8 MPa, respectively.

Fig. 16. Nonlinear results: Displacement and stress contours in the mid plane of the layered geometry.

[Note: The dashed lines represent the interfaces between "fiber" and "matrix" layers.]

x	y	u	v	w
0.4000E-05	0.0000E+00	-8.570E-09	0.000E+00	-1.110E-07
0.2828E-05	0.2828E-05	-7.417E-09	-7.866E-10	-7.670E-08
0.0000E+00	0.4000E-05	0.000E+00	4.212E-10	0.000E+00
0.0000E+00	0.2000E-05	0.000E+00	4.744E-10	0.000E+00
0.0000E+00	0.0000E+00	0.000E+00	0.000E+00	0.000E+00
0.2000E-05	0.0000E+00	-5.754E-09	0.000E+00	-5,529E-08
0.1662E-05	0.1662E-05	-4.977E-09	6.559E-11	-4.566E-08
0.6400E-05	0.6000E-05	-8.606E-09	0.000E+00	1.127E-07
0.4352E-05	0.6000E-05	-7.581E-08	0.000E+00	1.165E-08
0.2374E-05	0.6000E-05	-4.423E-08	0.000E+00	-8.734E-10
0.0000E+00	0.6000E-05	0.000E+00	0.000E+00	0.000E+00
0.0000E+00	0.5000E-05	-6.104E-09	0.000E+00	0.000E+00
0.5758E-05	0.0000E+00	-7.338E-08	0.000E+00	-1.852E-08
0.7868E-05	0.0000E+00	-4.542E-08	0.000E+00	2.906E-08
0.1040E-04	0.0000E+00	0.000E+00	0.000E+00	0.000E+00
0.1040E-04	0.1000E-05	0.000E+00	-6.449E-09	0.000E+00
0.1040E-04	0.2000E-05	0.000E+00	-3.823E-10	0.000E+00
0.7572E-05	0.3172E-05	-7.253E-09	-1.257E-09	7.897E-08
0.5300E-05	0.2056E-05	-5.966E-08	-1.788E-08	-8.362E-09
0.7814E-05	0.1517E-05	-4.802E-08	-1.064E-08	1.324E-08
0.4930E-05	0.3910E-05	-6.016E-08	-1.801E-08	7.548E-09
0.2505E-05	0.4427E-05	-4.760E-08	-1.052E-08	-1.185E-08
0.1040E-04	0.6000E-05	0.000E+00	0.000E+00	0.000E+00
0.8400E-05	0.6000E-05	-5.379E-09	0.000E+00	5.732E-08
0.1040E-04	0.4000E-05	0.000E+00	3.879E-11	0.000E+00
0.8738E-05	0.4338E-05	-4.497E-09	-2.502E-10	4.692E-08

Table 1: Computational results for the displacement components u, v and w (in meters) at various positions (x; y) in the mid plane z = 0.

		Linear Elastic				Elastic Fiber, Plastic Matrix			
		Fiber (MPa)		Matrix (MPa)		Fiber (MPa)		Matrix (MPa)	
		Min.	Max.	Min.	Max.	Min.	Max.	Min.	Max.
σ_{xx}	L	-2.10	0.64	-1.57	-1.06	-8.48	8.86	-0.87	-0.69
σ_{xx}	C	-10.62	15.68	-5.14	3.44	-38.92	52.85	-2.00	1.73
σ_{yy}	L	-23.06	-21.39	-1.04	-0.84	-32.42	-12.70	-1.01	-0.47
σ_{yy}	C	-12.55	0.53	-6.15	4.21	-15.91	8.51	-3.06	3.05
σ_{zz}	L	-75.75	-71.70	-2.41	-1.24	-104.53	-42.73	-1.72	-0.24
σ_{zz}	C	-24.20	42.39	-11.89	6.26	-144.81	148.45	-3.47	2.89
τ_{xy}	L	0.00	0.00	0.00	0.00	0.00	0.00	0.00	0.00
τ_{xy}	C	-1.55	2.17	-3.35	1.60	-6.20	7.30	-0.98	0.62
τ_{xz}	L	128.03	130.64	128.18	129.41	55.50	74.37	50.55	51.03
τ_{xz}	C	233.15	265.88	16.16	220.45	90.64	198.91	9.46	70.23
τ_{yz}	L	0.00	0.00	0.00	0.00	0.00	0.00	0.00	0.00
τ_{yz}	C	-9.49	11.98	0.78	110.12	-12.99	-38.81	0.50	37.27

Table 2: A comparative listing of maximal and minimal stresses at the mid-plane z = 0, for circular fibrous (C) and layered (L) geometries.